Modeling of an electrohydraulic lithotripter with the KZK equation

Michalakis A. Averkiou[a] and Robin O. Cleveland[b]
Applied Physics Laboratory, University of Washington, Seattle, Washington 98105

(Received 14 May 1998; accepted for publication 7 March 1999)

The acoustic pressure field of an electrohydraulic extracorporeal shock wave lithotripter is modeled with a nonlinear parabolic wave equation (the KZK equation). The model accounts for diffraction, nonlinearity, and thermoviscous absorption. A numerical algorithm for solving the KZK equation in the time domain is used to model sound propagation from the mouth of the ellipsoidal reflector of the lithotripter. Propagation within the reflector is modeled with geometrical acoustics. It is shown that nonlinear distortion within the ellipsoidal reflector can play an important role for certain parameters. Calculated waveforms are compared with waveforms measured in a clinical lithotripter and good agreement is found. It is shown that the spatial location of the maximum negative pressure occurs pre-focally which suggests that the strongest cavitation activity will also be in front of the focus. Propagation of shock waves from a lithotripter with a pressure release reflector is considered and because of nonlinear propagation the focal waveform is not the inverse of the rigid reflector. Results from propagation through tissue are presented; waveforms are similar to those predicted in water except that the higher absorption in the tissue decreases the peak amplitude and lengthens the rise time of the shock. [S0001-4966(99)04306-4]

PACS numbers: 43.25.Jh [MAB]

INTRODUCTION

Extracorporeal shock wave lithotripsy (ESWL) has been used successfully since 1980[1] to treat kidney and gall stones.[2] The noninvasive nature of this procedure has proven to be very attractive over its alternative method, surgical removal, even though the exact mechanism by which the shock wave fragments the stone is not clearly understood. In the case of kidney stones, ESWL is employed in about 85% of the encountered cases; for gall stones, it is used in about 20% of the cases, primarily in Europe. The first attempts to comminute human calculi with the use of acoustic energy are traced back to the early 1950s.[3] Since then, steady improvement in the application of this method has occurred,[4] and today ESWL is by far the method of choice.

ESWL involves the use of large amplitude acoustic shock waves that are generated extracorporeally and focused onto a stone within the body. Lithotripters typically have a high focusing gain so that pressures are high at the stone but substantially lower in the surrounding tissue. The positioning of the patient (alignment of stone with the lithotripter focus) is accomplished with fluoroscopy or ultrasonic imaging. Focusing is achieved geometrically, i.e., with ellipsoidal reflectors, concave focusing dishes, or acoustic lenses. The shock waves utilized have amplitudes of tens of Megapascals [a few hundred kilopascals] and durations of a few microseconds. Shock waves are typically fired at a 1-s pulse repetition rate.

The first mechanisms proposed for stone comminution were compressive failure[5] and spalling.[6] Compressive failure occurs when the large peak positive pressure of the shock wave enters the stone; if the applied stress exceeds the compressive strength of the material, failure will occur. Spalling is the process whereby the positive pressure enters the stone and reflects off the back surface of the stone. The acoustic wave is inverted upon reflection and the resulting tensile stress causes the material to fail (most solids are substantially weaker under tensile stress than compressive stress). A few years after lithotripsy was introduced, acoustic cavitation was suggested as an alternative mechanism for stone fragmentation.[7,8] Acoustic cavitation refers to the formation and subsequent implosive collapse of small cavities (bubbles) within a liquid. The collapse of cavitation bubbles can be violent enough to erode even the hardest metals used in ship propellers and turbine blades.[9] A fourth mechanism of stone failure that has recently been proposed is the process of dynamic fatigue.[10] In this scenario the incident shock wave need not exceed the static strength of the material, but simply cause the progressive development of microcracks in the material. Repetitive stress will fatigue the material (the cracks will grow) and eventually lead to catastrophic failure.

The side effects of ESWL were initially thought to be restricted to hematuria (blood in the urine).[1] However, there is now substantial evidence that ESWL leads to renal injury in a majority, if not all, treated kidneys.[11,12] The renal injury consists of primary damage to the vascular system seen as focal regions of hemorrhage at the focus and a fall in renal blood flow due to vasoconstriction with secondary effects resulting from ischemia.[13,14] The tissue equivalent of spalling occurs at air interfaces, such as in the lung and intestines, and has a damage threshold around 1 MPa;[15,16] however, in ESWL the shock wave is kept away from possible air pockets. Cavitation is also a possible mechanism for tissue damage. If cavitation bubbles have the ability to grow in tissue without significant restraint, then the subsequent bubble im-

[a]Present address: ATL Ultrasound, P.O. Box 3003, Bothell, WA 98041.
[b]Present address: Dept. of Aerospace and Mechanical Engineering, Boston University, Boston, MA 02215.

plosion would lead to tissue damage.[17] A third mechanism for tissue damage is shear, where small-scale inhomogeneities in the tissue distort the wavefront of the incoming shock wave, inducing a shear which can lead to destruction of the tissue.[18]

Before the issues of stone comminution and tissue damage are fully understood, it is necessary to know the acoustic field generated by a lithotripter. Measurements exist for lithotripsy shock waves in water. However, it is perhaps more important to know the acoustic field inside the body where it acts on both the tissue and the kidney stone. Numerical calculations have the potential for great utility in this situation because measurements are difficult to obtain in the body.

The electrohydraulic lithotripter accomplishes its focusing by means of a hemi-ellipsoidal reflector. A spark is discharged at the first focus, f_1, inside the reflector, which generates a shock wave that is reflected and focused at the second focus, f_2. Modeling of the acoustic field of an electrohydraulic lithotripter has been addressed before. Coleman *et al.*[19] used a 1-D version of the KZK equation (essentially the Burgers equation) to model focal waveforms. Diffractive effects were accounted for by assuming that the sound field behaved as a Gaussian beam. Christopher[20] solved the problem accounting for diffraction, absorption, and nonlinearity with the use of a nonlinear propagation model.[21] However, he found it necessary to artificially limit the peak negative pressure during calculations, justified by the fact that his predictions of peak negative pressure exceeded the expected tensile strength of water.

In this work we use the Khokhlov–Zabolotskaya–Kuznetsov (KZK) equation[22,23] to model the field of an electrohydraulic lithotripter outside the reflector. The equation accounts for diffraction (in the parabolic approximation), nonlinearity, and absorption. Results from the KZK equation have been compared with experimental measurements in the past, for continuous wave (CW) and pulsed propagation of focused and unfocused sound beams in water and glycerin, and was found to be in excellent agreement.[24–29]

A limiting factor on the KZK equation is the assumption of quasi-one-dimensional propagation, which manifests itself in the parabolic approximation of the diffraction. Indeed Tjøtta *et al.*[30] argue that the KZK equation is only appropriate for focused sound beams when the aperture radius a and focal length d are such that $a/d<0.5$, that is, the half-aperture is less than 16°. Physically it is argued that the discrepancy occurs because the parabolic approximation does not properly capture the edge wave behavior. The error increases in magnitude with the aperture angle. In the studies mentioned above focusing gains were moderate (less than 20). Hart and Hamilton[31] introduced a coordinate transformation in the frequency domain code that enabled them to consider gains as high as 70. In a previous work by one of the authors[32] the linear field of focused pistons of gains up to 120 and aperture angles up to 90° was considered. It was found that the KZK equation was consistent with O'Neil's exact solution[33] in the focal region for aperture angles up to 30°. In the results presented here the focusing gain was 24.5 and $a/d=0.62$ (a half-aperture angle of 32°). Although this would appear to be slightly outside the parameter space where the KZK equation is valid, the limitations given above were for a uniform focused piston source. As discussed below the ellipsoidal reflector is equivalent to a focused source with an amplitude shading that is approximately Gaussian. This means that the amplitude of the edge wave for an electrohydraulic lithotripter is significantly smaller than would occur with a uniformly focused piston source. Indeed focused Gaussian fields may be matched to focused uniform fields with a transformation that scales the Gaussian gains by a factor of 0.5 or $1/\sqrt{12}$[34,35] depending on the assumptions. Our gain of 24.5 is thus effectively an effective uniform piston gain of $12\cdot 25$ or less. The edge wave error induced by the parabolic equation is therefore much less than would otherwise be expected.

In Sec. I we present the theoretical model and its numerical solution. The method by which we model propagation within the reflector and initialize the code is described. In Sec. II we describe the experimental setup and the measurements performed. In Sec. III we present our results. The numerical results for linear propagation are compared with the exact on-axis solution by Hamilton.[36] We demonstrate that the parabolic approximation is indeed valid for the large aperture considered here. We then consider the effect of nonlinear propagation within the bowl. Comparisons with experimental data from a clinical lithotripter are shown. In our numerical results we show propagation curves for both the peak positive and peak negative pressures as well as time waveforms both on-axis and off-axis. We calculate the field for a lithotripter with a pressure release reflector. We also calculate the field for the case of propagation through tissue.

I. THEORETICAL MODEL

In this section we present a description of the theoretical model used (the KZK equation) and its numerical solution. The KZK equation is a quasi-one-dimensional model and is not appropriate for modeling propagation within the reflector where waves travel in both directions. Instead ray theory is used to model propagation within the bowl. The results from ray theory are used as initial conditions for the KZK equation for subsequent propagation outside the bowl.

A. KZK equation

Our model equation is an axisymmetric form of the KZK equation. We write it here in an integro-differential form in terms of the acoustic pressure p,

$$\frac{\partial p}{\partial z}=\frac{c_0}{2}\int_{-\infty}^{t'}\left(\frac{\partial^2 p}{\partial r^2}+\frac{1}{r}\frac{\partial p}{\partial r}\right)dt''+\frac{\delta}{2c_0^3}\frac{\partial^2 p}{\partial t'^2}+\frac{\beta}{2\rho_0 c_0^3}\frac{\partial p^2}{\partial t'}. \tag{1}$$

The variables are z the coordinate along the axis of the sound beam, r the radial distance from the beam axis, $t'=t-z/c_0$ a retarded time (based on the small-signal sound speed, c_0), δ the sound diffusivity,[37] β the coefficient of nonlinearity,[38] and ρ_0 the ambient density of the fluid. The three terms on the right hand side of Eq. (1) account for diffraction, absorp-

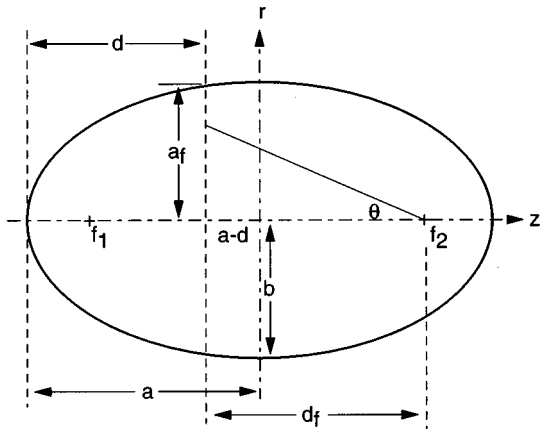

FIG. 1. Geometry of ellipsoidal reflector.

tion, and nonlinearity, respectively. As discussed by Cleveland *et al.*,[39] absorption and dispersion due to multiple relaxation phenomena can be augmented to the KZK equation.

The KZK equation is solved in the numerical code in dimensionless form. We introduce four normalized variables, $P=p/p_0$, $\sigma=z/d_f$, $\rho=r/a_f$, and $\tau=\omega_0 t'$, where, p_0 is the source pressure, d_f the focal length, a_f the aperture, and ω_0 a characteristic angular frequency. The KZK equation becomes:[40]

$$\frac{\partial P}{\partial \sigma}=\frac{1}{4G}\int_{-\infty}^{\tau}\left(\frac{\partial^2 P}{\partial \rho^2}+\frac{1}{\rho}\frac{\partial P}{\partial \rho}\right)d\tau'+A\frac{\partial^2 P}{\partial \tau^2}+N\frac{\partial P^2}{\partial \tau}. \quad (2)$$

The three dimensionless parameters that describe the relative importance of diffraction, absorption, and nonlinearity are:

$$G=z_0/d_f, \quad A=\alpha_0 d_f, \quad N=d_f/\overline{z}, \quad (3)$$

respectively. The first parameter, G, is the small-signal focusing gain, where $z_0=\omega_0 a_f^2/2c_0$ is the Rayleigh distance. The absorption parameter contains the thermo-viscous attenuation coefficient $\alpha_0=\delta\omega_0^2/2c_0^3$. In the nonlinearity parameter the term $\overline{z}=\rho_0 c_0^3/\beta\omega_0 p_0$ is the plane wave shock formation distance. The source condition appropriate for a uniform focused source is

$$P=f(\tau+G\rho^2)H(1-\rho) \quad \text{at } \sigma=0. \quad (4)$$

Equation (2) was solved numerically in the time domain using finite-difference operators to approximate the derivatives. The algorithm used was similar to that given by Lee and Hamilton[40] for unfocused, diverging sound beams except that a rectangular grid was used to accommodate the geometry of focused beams.[41]

B. Source condition for an electrohydraulic lithotripter

The KZK equation can only be applied to acoustic propagation from the aperture of the lithotripter's reflector (also referred to as the bowl). The evolution of the waves inside the bowl is considered here. A schematic of the ellipsoidal reflector is shown in Fig. 1. The foci of the ellipse are f_1 and f_2, and d is the distance from the edge to the point where the ellipse is truncated (the reflector is typically not a complete hemi-ellipsoid). The distance d_f and a_f are the effective focal length and source radius to be used with the KZK equation.

The ellipsoidal reflector has similar characteristics to a focused piston source and the pressure field at the mouth of the bowl is adapted from Eq. (4),

$$P=D(\rho)f(\tau+G\rho^2)H(1-\rho), \quad (5)$$

where $D(\rho)$ is the amplitude shading across the ellipse, $f(t)$ is the source waveform, and $G\rho^2$ is a phase term that effects the focusing of the bowl.

The shading function can be determined from the geometry of the ellipsoid. The surface of an ellipsoidal reflector is defined by

$$\frac{z^2}{a^2}+\frac{r^2}{b^2}=1, \quad (6)$$

where a and b are the major and minor axes of the ellipse. We define the eccentricity to be $\epsilon=\sqrt{1-(b/a)^2}$. The distance d measured from the tip of the ellipse to the exit plane. From geometry we find that the effective radius is

$$a_f=b\sqrt{1-(d/a-1)^2}, \quad (7)$$

and the effective focal length is

$$d_f=a(\epsilon+1-d/a). \quad (8)$$

Equations (7) and (8) are used as the equivalent focused piston parameters in Eq. (3). In these simulations the geometrical parameters were chosen to be: $a=13.80$ cm, $b=7.75$ cm, $\epsilon=0.8274$, $d=12.41$, $a_f=7.71$ cm, and $d_f=12.82$ cm. These values match those of the Dornier HM3 lithotripter which was the clinical machine on which we took measurements.

The directivity function at the mouth of the ellipse $D(\rho)$ can be derived from geometrical acoustics,[36]

$$D(\rho)=\cos(\theta)\Big/\left[1+\frac{4\epsilon\sin^2(\theta/2)}{(1-\epsilon)^2}\right], \quad (9)$$

where

$$\theta=\arctan\sqrt{\left[(1-\epsilon^2)\rho^2\frac{1-(d/a-1)^2}{(1+\epsilon-d/a)^2}\right]}. \quad (10)$$

For the ellipsoidal bowls used in lithotripters the eccentricity is typically $\epsilon\approx 0.8$. When $\epsilon=0$ (spherical bowl) then $D(\rho)=1$ and Eq. (5) reduces to Eq. (4), i.e., a uniform focused piston source. As ϵ increases, the directivity function is no longer unity and is effectively an amplitude shading function (source apodization). Thus we model the ellipsoidal reflector as a focused source with radius a_f, focal length d_f, and with amplitude source shading defined by $D(\rho)$. For $\epsilon\approx 0.8$ the amplitude at the edge of the aperture is approximately 10% of the amplitude on-axis. The significantly reduced amplitude of the edge wave is what allows us to use the KZK equation beyond its ordinary limit.

Hamilton[36] gives an analytic solution for the linear on-axis field of a spherical wave reflected by an ellipsoidal reflector that accurately models diffraction. We use his expression to verify our axial numerical results for a linear case.

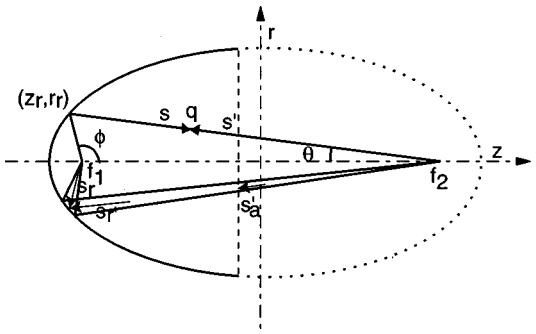

FIG. 2. Geometry of rays within the ellipsoidal reflector.

C. Ray theory within the bowl

The equations shown above for the acoustic field at the mouth of the reflector, although compact, are not easily adapted to account for finite-amplitude effects within the bowl. It is therefore necessary to develop the expressions for ray theory within the bowl. First, we consider the case of small-signal propagation. We assume that propagation is governed by geometrical acoustics, that is, diffraction is negligible within the bowl.

The spark source is assumed to produce a spherically spreading wave. The ellipsoidal reflector is such that spherically spreading waves generated at f_1 reflect off the ellipsoidal bowl, and spherically converge on f_2. Figure 2 shows one set of rays for the ellipsoidal reflector. A ray departs f_1 at an angle ϕ with respect to the z-axis. It intersects with the reflector at location (z_r, r_r) and converges on f_2 along a line at an acute angle of θ to the z-axis. At a given point q on the ray we define s to be the path length from f_1 to q, and s' to be the distance from f_2 to q. By the geometry of the ellipse $s+s'=2a$. The intersection of the outgoing rays and the ellipse occurs at $r_r=a(1-\epsilon^2)\sin\phi/(1-\epsilon\cos\phi)$, $z_r=-a(\epsilon-\cos\phi)/(1-\epsilon\cos\phi)$. The angle θ for the reflected ray is given by $\theta=\tan^{-1}[r_r/(\epsilon a-z_r)]$ [see also Eq. (10)]. The distance from f_2 to the reflector is given by $s_r'=a(1-\epsilon^2)/(1-\epsilon\cos\theta)^2$, and the distance from f_1 to the reflector is $s_r=2a-s_r'$.

The shading can now be calculated. Consider a ray that starts a distance s_0 from f_1, the ray tube area along the path to the reflector is $A_1(s)=A_0(s/s_0)^2$, where A_0 is the initial ray tube area. The ray tube area along the reflected ray is $A_2(s)=k(s'/s_r')^2$, recall that $s'=2a-s$. The constant k can be determined by equating the ray tube areas A_1 and A_2 at the reflector and $k=A_0(s_r/s_0)^2$. The general expression for the ray tube area within the bowl is therefore

$$A(s)=\begin{cases} A_0\left(\dfrac{s}{s_0}\right)^2 & s\leqslant s_r \\ A_0\left(\dfrac{s_r}{s_0}\right)^2\left(\dfrac{2a-s}{s_r'}\right)^2 & s>s_r. \end{cases} \tag{11}$$

The ray tube area at the aperture $s=s_a$ is therefore

$$A(s_a)=\frac{s_1(2a-s_a')}{s_2 s_0}A_0,$$

where $s_a'=((1+\epsilon)a-d)/\cos\theta$ is the distance from f_2 to the aperture.

Therefore for the case of linear propagation the waveform at the aperture is a scaled version of the waveform at s_0, where the scaling factor is $\sqrt{A_0/A(s_a)}$. This expression agrees with the directivity function given in Eq. (9). For the case of a nonrigid reflector, with pressure reflection coefficient R, the expression becomes $R\sqrt{A_0/A(s_a)}$.

The analysis can now be extended to include nonlinear effects. To achieve this it is necessary to further assume that the is no self-interaction between rays, that is, nonlinear effects are restricted to distortion along ray tubes given by linear theory. It is also assumed that nonlinear distortion within the bowl can be accounted for by weak shock theory.[42]

We assume that the spark generates a triangle wave of peak amplitude $\hat{p}_0$ and duration T_{h0}. A triangle wave is a good approximation to the waveform generated by an explosive source[43] such as in an electrohydraulic lithotripter. Although we use a triangular waveform it is possible to generalize the approach to the evolution of shock waves followed by an arbitrary waveform.[44] For a plane triangular wave, weak shock theory predicts that the peak amplitude and duration of the pulse will vary as

$$\hat{p}=\frac{\hat{p}_0}{\sqrt{1+ax}}, \tag{12}$$

$$T_h=T_{h0}\sqrt{1+ax}, \tag{13}$$

where x is the propagation distance and $a=\beta\hat{p}_0/\rho_0 c_0^3 T_{h0}$.

For the shocks inside the bowl the waves initially spread spherically outward, reflect off the ellipsoidal bowl, and then spherically converge. For finite-amplitude waves in a slowly varying ray tube modified versions of Eqs. (12) and (13) can be used to describe the triangle waves where the real distance x is replaced by the ''distortion distance'' $\tilde{x}$.[45] The distortion distance for an arbitrary ray tube in a homogeneous medium is

$$\tilde{x}=\int_{s_0}^{s}\sqrt{\frac{A(s_0)}{A(s')}}\,ds', \tag{14}$$

where s is a distance along the ray, s_0 is the initial location along the ray, and A is the ray tube area.

When the expression for the ray tube area is substituted into Eq. (14), the effective nonlinearity distance within the bowl is

$$\tilde{x}(s)=\begin{cases} s_0\ln\left(\dfrac{s}{s_0}\right) & s\leqslant s_r \\ s_0\ln\left(\dfrac{s_r}{s_0}\right)-s_r'\dfrac{s_0}{s_r}\ln\left(\dfrac{2a-s}{s_r'}\right) & s>s_r. \end{cases} \tag{15}$$

The effective nonlinearity distance at the aperture is

$$\tilde{x}_a=s_0\ln(s_r/s_0)-s_r'(s_0/s_r)\ln[(2a-s_a')/s_r'].$$

The inclusion of the reflection coefficient simply modifies the second term of the nonlinear distortion distance and one obtains

$$\tilde{x}_a = s_0 \ln(s_r/s_0) - R s_r'(s_0/s_r)\ln[(2a - s_a')/(s_r')]. \quad (16)$$

The expressions describing the peak pressure and duration of the triangle wave at the aperture are therefore

$$\hat{p}_a = R \frac{s_r(2a - s_a')}{s_r' s_0} \frac{\hat{p}_0}{\sqrt{1 + a\tilde{x}_a}}, \quad (17)$$

$$T_{ha} = T_{h0}\sqrt{1 + a\tilde{x}_a}. \quad (18)$$

These expressions can be used to consider the effects of nonlinear distortion within the ellipsoidal reflector. Coleman reported that the waveform measured on-axis at the aperture of a Dornier HM3 was a triangle wave with amplitude 8 MPa.[46] Coleman later reported the aperture waveform to be triangular with a peak amplitude of approximately 5 MPa and a duration of 3.75 μs.[19] For our calculations we assumed that the waveform at the aperture was a triangle wave of peak pressure 6.54 MPa (between the reported values) and duration 4 μs. The selection of 6.54 MPa was chosen because it was approximately the average of the values reported by Coleman and it gave a nonlinearity parameter [Eq. (3)] of exactly 1.4. Using linear theory to backpropagate to 1 cm away from the spark, the initial condition becomes a triangle waveform of amplitude 7.91 MPa and 4-μs duration. Figure 3 shows the amplitude shading and the aperture waveforms on the axis and the edge of the ellipsoidal reflector compared to linear theory. Nonlinear distortion within the bowl leads to a loss in amplitude for the weak shock theory case which is strongest on axis (6.06 MPa vs 6.54 MPa). Nonlinear effects also lead to an elongation of the waveform; again this is most marked on-axis (4.32 μs vs 4 μs). The latter distortion will produce a change in the curvature of the leading wavefront which should produce a defocusing effect at f_2. However, for this case the effects of nonlinear distortion in the bowl are very small.

Christopher also used a triangle wave as an initial waveform. In his calculations he assumed that 1 cm from f_1 the waveform was a triangle wave of amplitude 40 MPa and duration 2 μs. Figure 4 compares the predicted waveforms at the mouth of the reflector for linear and weak shock theory for this initial condition. On-axis, weak shock theory predicts an amplitude of 20.2 MPa compared to 30.7 MPa for linear theory. The duration on-axis is 3.27 μs for weak shock theory and 2 μs for linear theory. For this source condition nonlinear distortion significantly affects the propagation problem, producing a large decrease in amplitude and defocusing of the wavefront. Christopher assumed linear propagation within the bowl, but his model also accounted for diffraction within the bowl. However, as discussed below, the acoustic field predicted at the mouth of the ellipsoid by geometrical acoustics agrees well with predictions with the exact on-axis linear solution which includes diffraction.

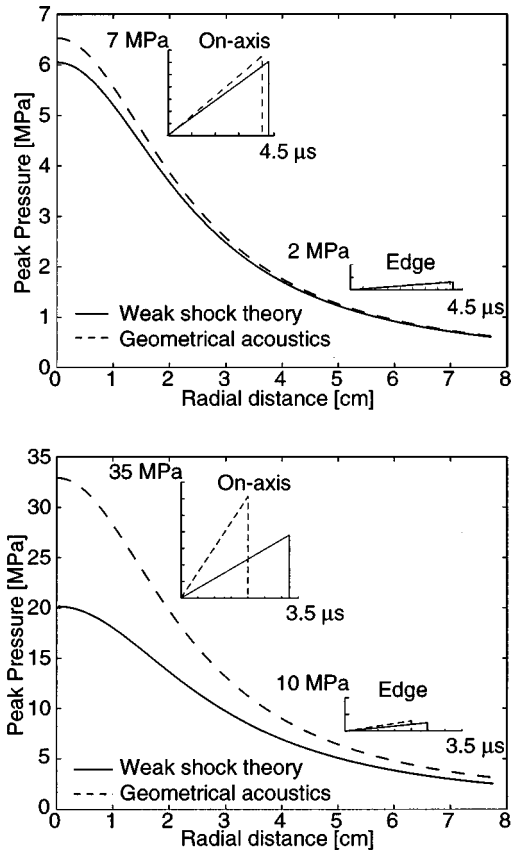

FIG. 3. Amplitude shading across the bowl mouth and waveforms both on-axis and at the edge of the bowl. (a) Comparison of linear geometrical acoustics and weak shock theory for propagation in the bowl for amplitudes used in this paper. When nonlinear effects are accounted for there is a small reduction in amplitude and pulse elongation; the effect is largest on-axis but is not significant for these pressures. (b) Comparison of linear geometrical acoustics and weak shock theory for the initial conditions used by Christopher. Nonlinear distortion significantly reduces the amplitude of the pulse and elongates it, with the greatest effect being on-axis.

II. EXPERIMENTAL SETUP

Pressure measurements were taken in an unmodified Dornier HM3 lithotripter at Methodist Hospital, Indianapolis, IN. A replaceable PVDF membrane hydrophone (no. 702-031, Sonic Industries, Hatsboro, PA) was used to capture the shock waves generated by the lithotripter. Individual membranes were supplied with a calibration value which is reported to be within ± 1.5 dB over the frequency range 1–20 MHz. We confirmed the calibration over the range of 2–20 MHz by comparilson with a Marconi PVDF hydrophone (type Y-33-7611, GEC-Marconi, Chelmsford, UK) calibrated at the National Physical Laboratory (Teddington, UK). We were not able to obtain a calibration below 1 MHz but, assuming that the response remains moderately flat, we estimate the error in the measured pressure to be $\pm 20\%$. Waveforms were recorded on a digital oscilloscope (Tektronix, Beaverton, OR) and downloaded to a computer using LabVIEW (National Instruments, Austin, Texas).

The lithotripter was placed in patient-ready condition—its water bath filled with standard Dornier degased, softened water at 37 °C. We used refurbished electrodes (Service Trends, Kennesaw, GA) between shot 50 and 2000 with a voltage setting of 18 kV. The Dornier water has high conductivity (700 μS/cm) that adversely affects the response of the PVDF membrane; the hydrophone requires a conductivity of less than 5 μS/cm. We placed the shock wave hydrophone inside a small plastic tank (dimensions $22\times32\times30$ cm) of deionized water inside the HM3 water bath. The bottom surface of the tank, where the shock wave enters, was

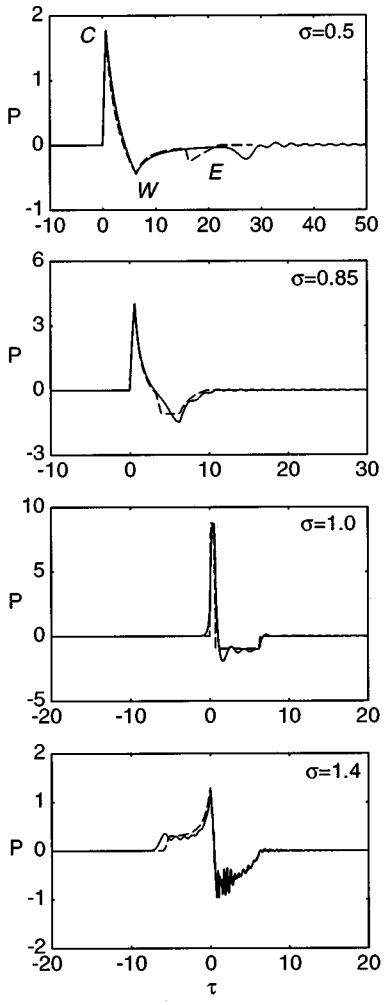

FIG. 4. Comparison between numerical results from the KZK equation (solid line) and Hamilton's exact linear analytical solution (dashed line) for time waveforms along the axis of an ellipsoidal reflector. In the pre-focal region the edge wave of the numerical solution is delayed.

fitted with a thin sheet of low density polyethylene. The polyethylene sheet had a negligible effect on the shock wave.

The hydrophone was located at the focus of the lithotripter by placing a small radio-opaque marker on the active portion of the membrane so that it could be visualized using the fluorography system associated with the HM3. The membrane was moved using the hydraulic gantry system of the HM3 until the marker was at the focal point as determined by the crosshairs on the fluoroscope screens. The marker was removed for shock wave measurements.

The hydrophone was moved to other locations by the hydraulic gantry system. Location was determined by means of two masks placed on the fluoroscopic screens. The masks had calibrated grids drawn on them that were aligned with the blast path of the lithotripter. At least ten measurements were taken at each location and the PVDF membrane and polyethylene sheet were cleared of bubbles after every shot.

III. RESULTS

Our numerical and experimental results are shown in this section. We compared results with linear theory for an ellipsoidal reflector to demonstrate that the application of the initial conditions for the KZK code was correct. Next we compared computed lithotripsy waveforms in water with experimentally measured shock waves. Finally, the code was used to predict the acoustic field for two cases: (1) a lithotripter with a pressure release reflector and (2) a standard lithotripter but with the shock waves propagating in tissue.

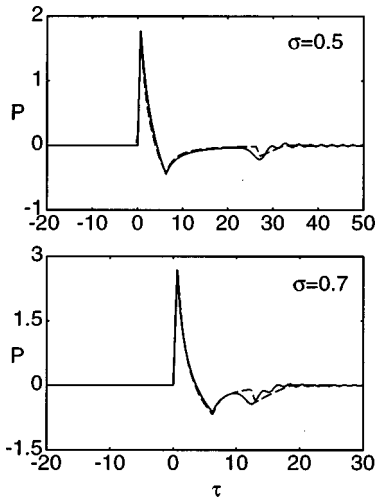

FIG. 5. Comparison between the numerical simulation (solid line) and the modified (according to the paraxial approximation) exact linear analytical solution by Hamilton (dashed line) for time waveforms along the axis of an ellipsoidal reflector. The arrival times of the edge waves agree.

A. Comparison with linear theory

Figure 4 shows a comparison between numerical results for linear propagation along the axis of the ellipsoidal reflector and the exact analytical solution of Hamilton.[36] The source condition was the triangular pulse discussed above with a rise time of 400 ns and duration of 4 μs. In the figures that follow we used the normalized axial distance $\sigma = z/d_f$ with $\sigma = 1$ being the ellipsoidal reflector focus, f_2. Recall that the effective ellipsoid radius and focal distance used by the Dornier HM3 are $a_f = 7.7$ cm and $d_f = 12.8$ cm, respectively. In Fig. 4 at $\sigma = 0.5$ we indicate the three main parts of the waveform: the center wave (or direct wave) denoted as *C*, the edge wave (or diffracted wave) denoted as *E*, and the wake denoted as *W*. A discussion of these three wave components may be found in Ref. 36. In the near field, note that the edge wave in the KZK solution lags behind that of the exact solution. This is an inherent limitation of the parabolic approximation in the diffraction term.

We illustrate the effect of the parabolic approximation on the solution by applying the parabolic approximation to the exact analytical solution. This was done by replacing the distance to the edge of the aperture $R_e = \sqrt{z^2 + a^2}$ by the first two terms of its binomial expansion $R_e \approx z(1 + 0.5(a/z)^2)$. This is effectively what happens when the parabolic approximation is applied to the wave equation. Figure 5 shows that the comparison between the numerical results and the ''parabolic'' analytical solution is better. This suggests that the main difference between our model and the exact solution is in terms of the edge wave prediction due to the parabolic approximation. In the rest of the axial ranges we have good agreement between the numerical and the analytical solution.

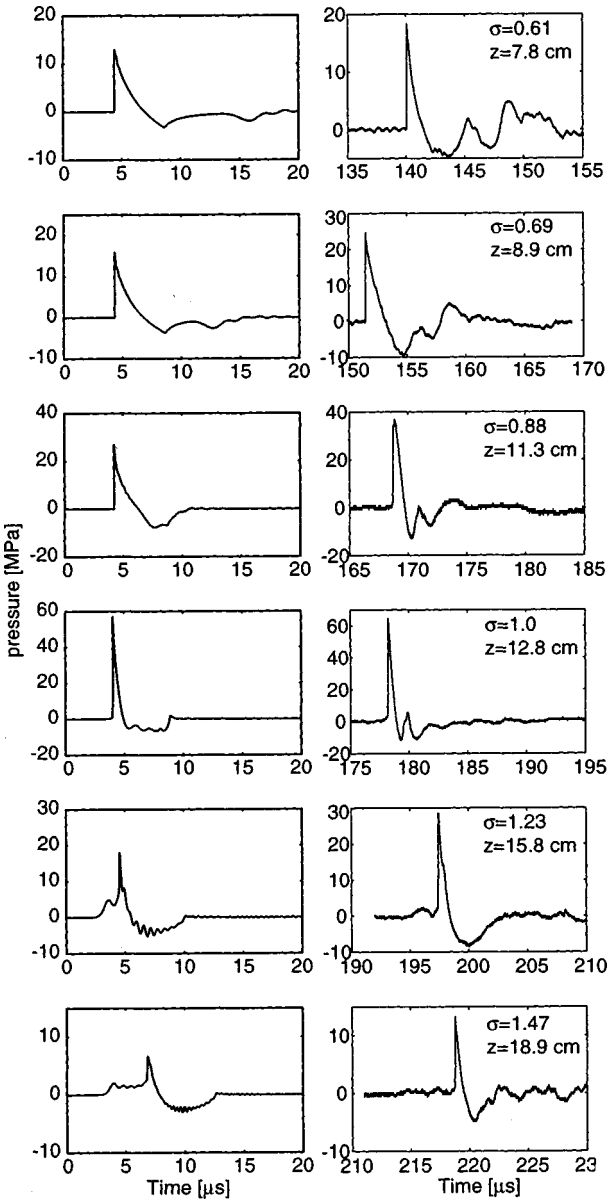

FIG. 6. Comparison between measured lithotripter shock waves (right column) and the numerical simulation (left column) for $A=2.6\times10^{-3}$, $N=1.4$, and $G=24.5$, along the axis of the electrohydraulic lithotripter.

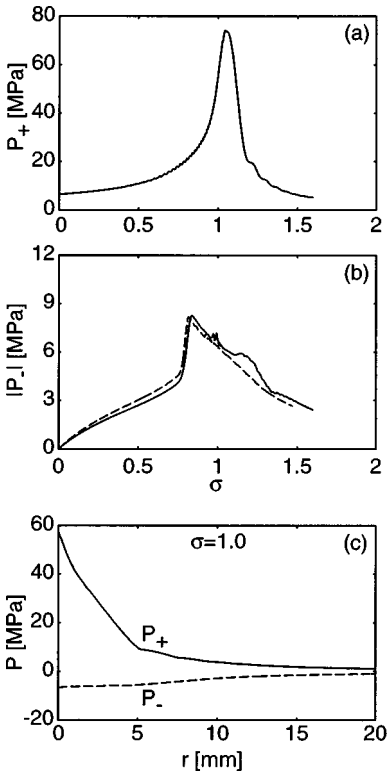

FIG. 7. Propagation curves for P_+ (a), $|P_-|$ (b), and beam patterns at $\sigma=1$ (c), for the numerical results shown in Fig. 6. The maximum of P_+ occurs just after the focus where as $|P_-|$ reaches a maximum pre-focally. Dashed lines in (b) show numerical results calculated with 5000 points per cycle.

The ripples at $\sigma=1.4$ are a Gibb's-type phenomenon, and they can be removed by finer discretization at the expense of longer run times.

B. Comparison with experiment

Results of calculations for the HM3 lithotripter were compared with data measured in the Dornier HM3 lithotripter at Methodist Hospital, in Fig. 6. The water parameters used for the numerical solution were α_0 ($f=0.25$ MHz) $=0.0016$Np/m, $\beta=3.5$, $\rho_0=1000\,\mathrm{kg/m^3}$, and $c_0=1485\,\mathrm{m/s}$. The source condition used was the same triangular pulse used in Sec. III A and the exit plane pressure amplitude was $p_0=6.54\,\mathrm{MPa}$. The absorption and nonlinearity parameters [as defined in Eq. (3)] were $A=2.6\times10^{-3}$ and $N=1.4$, and the focusing gain was $G=24.5$. For the diffraction calculation the step in the radial direction was such that the source radius was broken into 300 points. The triangular time waveform at the exit plane was sampled at 316 points per cycle (the duration of the triangular waveform being one cycle). Distance was measured from the ellipse exit plane and the distance to the focus was $d_f=12.82\,\mathrm{cm}$. The comparisons started at $z=7.8\,\mathrm{cm}$ (5-cm pre-focal) and extended out to $z=15.8\,\mathrm{cm}$ (3-cm post-focal).

At close range ($\sigma=0.61$) the numerical prediction for the edge wave was not very accurate; as discussed in the previous section, the calculated edge wave arrives delayed. Closer to the focus ($\sigma=0.88$) there was much better agreement for the arrival of the edge wave. At the focus ($\sigma=1$) the waveforms were in good agreement and the peak positive pressure was about 60 MPa in both the prediction and the measurement. However, the code predicted a significantly longer negative tail than was measured. The discrepancy may be due to an inherent limitation of the PVDF hydrophone to measure large negative pressures in water. Wurster *et al.*[47] claim that PVDF membranes do not properly capture the peak negative pressure of lithotripsy waveforms and underestimate the duration of the negative tail by a factor of 2. In the post-focal region ($\sigma>1$) the edge wave arrived before the center wave and it is seen as a small precursor to the shock wave in both the predicted and measured waveforms. Considering the great variability of waveforms measured in spark-discharge-type lithotripters, the agreement between the measured and predicted waveforms is good.

In Fig. 7(a) and (b) predictions for the axial peak-positive pressure (P_+) and the magnitude of the peak-negative pressure ($|P_-|$) are shown. The highest positive pressure was about 80 MPa and occurred close to the geo-

metric focus. However, the largest negative pressure was much lower (about 10 MPa) and occurred at $\sigma=0.84$ (2.0 cm in front of the focus). This result was in agreement with other measurements of the HM3.[48] If cavitation is shown to be a major mechanism in stone comminution then the positioning of patients may need to be adjusted to place the stone in a pre-focal region where cavitation activity would be strongest. The dashed line in Fig. 7(b) was calculated with 5000 points per cycle to demonstrate that the ripples in the solid line (316 points per cycle) were an artifact. In Fig. 7(c) P_+ (solid line) and P_- (dashed line) in the transverse direction at $\sigma=1$ are shown which indicate the radial extent of the lithotripsy field. The 6-dB beam width for P_+ was only 2.6 mm and for P_- was 9 mm. The magnitude of the negative pressure was above 1 MPa for a radial distance of 2 cm.

C. Pressure release bowl

Commercial electrohydraulic lithotripters use an ellipsoid made of brass or aluminum; both materials are acoustically hard compared to water, and may be modeled as rigid reflectors. Here we consider an ellipsoid that is made of an acoustically soft material, that is, it appears to be a pressure release reflector. In the numerical model the pressure release reflector was implemented by inverting the waveforms at the mouth of the ellipse. This was valid for our simulations because, as discussed above, the effect of nonlinear distortion within the bowl for our aperture conditions was almost negligible. If shock wave propagation in water was a linear process, then the waveforms from a lithotripter with a pressure release reflector would be the inverse of the results shown in Fig. 6. However, the high amplitudes utilized result in nonlinear effects and the calculated waveforms, shown in Fig. 8, were quite different from the waveforms calculated for a rigid reflector. At a range $\sigma=0.7$ the waveform resembled an inverted replica of the waveform obtained with a rigid reflector, but the center wave was steepening in the reverse direction and thus it had a slower decay time. The rest of the calculated waveforms did not resemble those of the rigid reflector. The maximum peak-positive pressure at the focus ($\sigma=1$) was about 30 MPa, considerably lower than that of the rigid reflector. The magnitude of the peak-negative pressure was about 25 MPa, considerably higher than the rigid reflector.

In Fig. 9 the variation of P_+ and $|P_-|$ along the ellipsoid axis is shown. Both P_+ and $|P_-|$ were maximized close to the geometric focus. The magnitude of the negative pressure was considerably greater than the positive pressure from the source all the way to the focus. Recently, Bailey[49,50] performed experiments with pressure release reflectors. His measured waveforms appear to be close to those calculated except that the magnitude of the negative pressures never exceeded 15 MPa. Two possible reasons for the discrepancy are that the hydrophone was not capable of measuring the large negative pressure (as discussed above), and that the reflector used in the experiments had a reflection coefficient $R=-0.88$ and our model assumed a perfect pressure release reflector $R=-1$.

We note that, despite the large negative pressures generated by the pressure release reflector, Bailey found that cavitation damage (as measured by pitting of metal foils) was significantly less than the cavitation damage of the rigid reflector. It was observed that the small pitting from the pressure release reflector was spread over a wider area than that

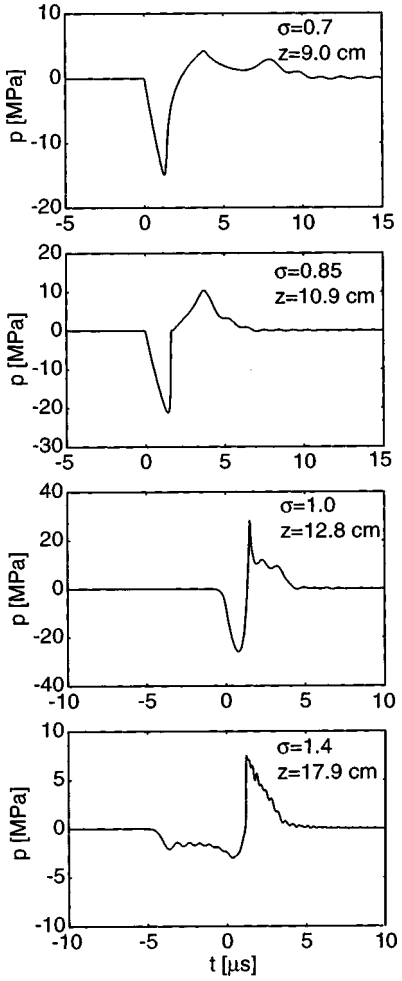

FIG. 8. Theoretical predictions for shock waves along the axis of a lithotripter with a pressure release reflector for $A=2.6\times10^{-3}$, $N=1.4$, and $G=24.5$. The waveforms are not simply inverted replicas of the waveforms shown in Fig. 6.

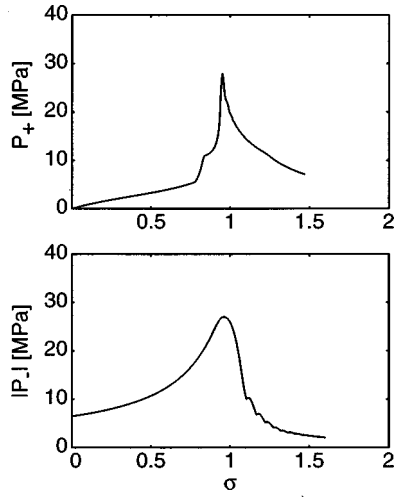

FIG. 9. Propagation curves for P_+ and $|P_-|$ for the pressure release reflector. Both curves have a maximum at the focus.

from the rigid reflector; but the conclusion was that the pressure release waveform produced minimal cavitation damage.[51] It appeared that the trailing positive spike in the pressure release waveform prematurely squashed cavitation bubbles and prevented the violent collapse that occurs for bubbles excited by the waveform of the rigid reflector.

D. Propagation in tissue

The results presented above are relevant for validating the numerical predictions with measurements in water. A powerful application of the code is the ability to predict the propagation of lithotripsy shock waves through tissue. The approach taken here was simplistic but the model has the potential to be used in a much more complicated way. Tissue was modeled as a homogeneous thermoviscous fluid where values for the absorption, the sound speed, the density, and the coefficient of nonlinearity were chosen to be representative of tissue in general. In addition, we assumed that all propagation took place in this approximate tissue model (no water path). It is possible to extend the numerical model to account for both propagation through layers of tissue with different parameters, and more realistic absorption using multiple relaxation processes.[39]

The parameters used for a model tissue were α_0 ($f=0.25\,\mathrm{MHz}$)$=1.52\,\mathrm{Np/m}$ (deduced from a nominal value of 7 Np/m/MHz and adjusted with a $f^{1.1}$ frequency dependence to $f=0.25\,\mathrm{MHz}$), $\rho=1000\ \mathrm{kg/m^3}$, $c=1520\,\mathrm{m/s}$, and $\beta=5.5$. The normalized absorption and nonlinearity parameters used in the numerical code were $A=0.195$ and $N=2.05$. The exit plane pressure amplitude remained the same as for the run in water, i.e., $p_0=6.54\,\mathrm{MPa}$. The calculated waveforms are shown in Fig. 10; the effect of the increased absorption acted as a low-pass filter and smoothed the waveforms. The higher absorption lead to peak amplitudes that were considerably lower than those for the waveforms in water (Fig. 6). At the focus, $\sigma=1$, the peak-positive pressure was 38% and the peak-negative pressure was 86% of the values in water. The peak-positive pressure P_+ was reduced more than $|P_-|$ because the amplitude of the peak-positive pressure is more sensitive to the presence of high frequency components than the peak-negative pressure. The Gibb's-type oscillations in the post-focal region were removed as a result of the absorption low-pass filtering. The shock wave rise time at the focus was 242 ns (calculated as the time to go from 10% to 90% of peak amplitude) and at $\sigma=1.1$ was 331 ns. For comparison, in water at $\sigma=1$ the estimated rise time was less than 1 ns but this estimation was somewhat limited by the discretization of the code. In the right hand side column off-axis waveforms are shown at the axial range $\sigma=1.0$. The pressure amplitude was greatly reduced off-axis and the shock wave rise time increased. At a distance of $\rho=0.15$ (12 mm) the waveform looked like a sinusoid and the amplitude was less than 3 MPa.

Figure 11 shows axial propagation curves for P_+ and $|P_-|$ in tissue. The major features here are that P_+ is maximized just after the focus and $|P_-|$ is maximized pre-focally, both traits were also seen in water simulations in Fig. 7. In Fig. 11(c), the transverse variation of P_+ and P_- is shown at a range $\sigma=1.0$. Both P_+ and $|P_-|$ retain relatively high

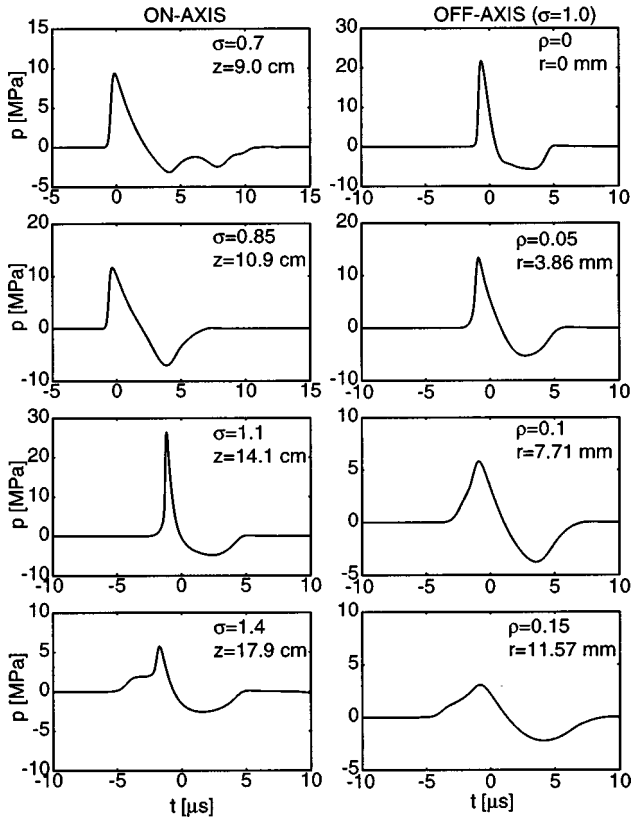

FIG. 10. Theoretical predictions for lithotripter shock waves in tissue with $A=2.6\times10^{-3}$, $N=1.4$, and $G=24.5$. The left-hand column shows axial waveforms and the right hand column shows radial waveforms (at the focus). The extra absorption in tissue smooths the waveforms, reducing the peak pressures and increasing the rise time.

amplitudes up to a range of 5 mm and cavitation activity should be monitored in that area. Cavitation activity may also be present up to (but not limited to) a range of 20 mm where $P_+=1.2\,\mathrm{MPa}$ and $P_-=-1.0\,\mathrm{MPa}$. The width of the focal spot (as defined by the 6-dB points) is broader by 70% in tissue than in water. The extra absorption in the tissue removes high frequency components and prevents tight focusing and results in a broader beam.

The predicted *in vivo* pressure field is in good agreement with measurements made in pigs of shock waves generated by an HM3.[52] The *in vivo* measurements indicated a 30% reduction in the peak-positive pressure at the focus. The calculations presented here predicted a 62% reduction in peak pressure but this was for propagation through 12.8 cm of tissue in pig measurements, the tissue propagation path was on the order of 6 cm. It is reasonable to expect the calculation to underestimate the peak pressure because more absorption was included. The *in vivo* rise time was measured to be on the order of 100 ns, which was longer than measured in water. The predicted rise time in tissue was 240 ns, also longer than predicted in water. The presence of the extra absorption would also account for the predicted rise time being longer than the measured rise time. The width of the focal spot *in vivo* was measured to be 20 mm, compared to 12 mm in water; a broadening of 67% very close to that predicted with this model.

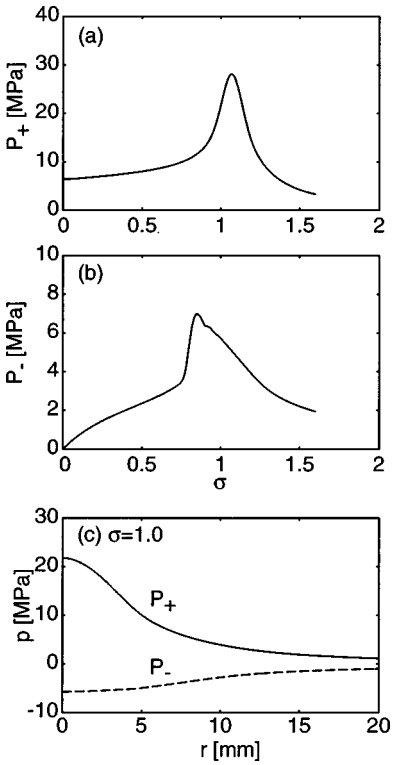

FIG. 11. Propagation curves and beam profiles for P_+ and $|P_-|$ for lithotripsy shock wave propagation in tissue. In this case, P_+ peaks post-focally indicating self-defocusing.

IV. CONCLUSION

The KZK equation was successfully used to model the acoustic field of an electrohydraulic lithotripter from the reflector exit plane to f_2 and beyond. The use of linear geometrical acoustics within the bowl was found to be adequate for exit plane pressures of about 7 MPa which result in focal pressures of about 60 MPa. For higher exit plane pressures, weak shock theory within the bowl is necessary. Comparisons of axial waveforms captured with a hydrophone in water with simulations from the KZK model showed good agreement. Possible reasons for the amount of discrepancy between experiment and simulation are that the model neglected the effects of masking of the aperture wave by the spark plug or the gas bubble at f_1. Also the model neglected the effect of spark variability at f_1. From both the model and the measurements it was found that the magnitude of the peak-negative pressure of the lithotripter shock wave was maximized prefocally. The model was also used to propagate an inverted shock wave that would be formed by a pressure release reflector. Our simulation results compared favorably with recent experimental results. According to our simulation, this type of reflector may result in negative pressures of up to 25 MPa. However, the structure of the focal waveform suggests that the resulting cavitation field is weaker than that of rigid reflectors.

Finally, modeling of propagation through tissue demonstrated the effects of increased absorption. The absorption acted as a low-pass filter; it increased the shock rise time and reduced the peak-positive pressure. In addition, the loss of the high frequency energy to absorption meant that the shock did not focus quite as tightly in tissue as it did in water. The code neglected the effects of refraction between layers of tissue and small-scale tissue inhomogeneities which could further broaden the size of the focal spot. The magnitude of the negative pressures in the tissue remained above 1 MPa for a transverse distance up to 20 mm from the axis (40 mm in diameter), as wide as a kidney. This suggests the extent of the area around the stone that may be subject to cavitation-type adverse bioeffect.

Further investigation is needed to correlate cavitation bioeffects with predicted and measured lithotripsy pressures. The present code appears to be an excellent tool for understanding the acoustic field generated by an electrohydraulic lithotripter both in water and in tissue.

ACKNOWLEDGMENTS

This work was funded by the National Institutes of Health through Grant No. DK43881. The help of Dr. M. F. Hamilton with theoretical aspects of this work is gratefully acknowledged. We also thank Drs. A. P. Evan and J. A. McAteer for providing access to the HM3 lithotripter at Methodist Hospital and for technical assistance. Cleveland acknowledges support of the Acoustical Society of America through the 1995/96 F.V. Hunt Fellowship.

[1] C. Chaussy, W. Brendel, and E. Schmiedt, ''Extracorporeally induced destruction of kidney stones by shock waves,'' Lancet **II**, 1265–1268 (1980).
[2] T. Sauerbruch, M. Delius, G. Paumgartner, J. Holl, O. Wess, W. Weber, and W. Brendel, ''Fragmentation of gallstones by extracorporeal shock waves,'' N. Engl. J. Med. **314**, 812–822 (1986).
[3] H. Lamport, H. F. Newman, and R. D. Eichhorn, ''Fragmentation of biliary calculi by ultrasound,'' Fed. Proc. **9**, 73–74 (1950).
[4] M. Delius and W. Brendel, ''Historical roots of lithotripsy,'' J. Lith. and Stone Disease **2**, 161–163 (1990).
[5] C. Chaussy, *Extracorporeally Shock Wave Lithotripsy: New Aspects in the Treatment of Kidney Stone Disease* (S. Karager, Basel, 1982).
[6] M. Delius, W. Brendel, and G. Heine, ''A mechanism of gallstone destruction by extracorporeal shock waves,'' Naturwissenschaften **75**, 200–201 (1988).
[7] A. J. Coleman, J. E. Saunders, L. A. Crum, and M. Dyson, ''Acoustic cavitation generated by an extracorporeal shockwave lithotripter,'' Ultrasound Med. Biol. **13**, 69–76 (1987).
[8] L. A. Crum, ''Cavitation microjets as a contributory mechanism for renal calculi disintegration in ESWI,'' J. Urol. (Baltimore) **140**, 1587–1590 (1988).
[9] L. A. Crum, ''Acoustic cavitation,'' 1982 Ultrasonics Symposium Proceedings (IEEE), Vol. 1, pp. 1–11.
[10] B. Sturtevant, ''Shock wave physics of lithotripters,'' in *Smith's Textbook of Endourology*, edited by A. D. Smith, G. H. Badlani, R. V. Clayman, G. H. Jordan, L. R. Kevoussi, J. E. Lingeman, G. M. Preminger, and J. W. Segura (Quality Medical Publishing, St Louis, MO, 1996), pp. 529–552.
[11] J. V. Kaude, C. M. Williams, M. R. Millner, K. N. Scott, and B. Finlayson, ''Renal morphology and function immediately after extracorporeal shock-wave lithotripsy,'' Am. J. Roentgenol. **145**, 305–313 (1985).
[12] A. P. Evan and J. A. McAteer, ''*Q*-Effects of shock-wave lithotripsy,'' in *Kidney Stones: Medical and Surgical Management*, edited by F. Coe, C. Pak, and G. M. Preminger (Raven, New York, 1996), pp. 549–570.
[13] A. P. Evan, L. R. Willis, B. Connors, G. Reed, J. A. McAteer, and J. E. Lingeman, ''Shock wave lithotripsy induced renal injury,'' Am. J. Kidney Disease **17**, 445–450 (1991).
[14] L. R. Willis, A. P. Evan, B. Connors, and J. E. Lingeman, ''Relationship between kidney size and acute impairment of renal hemodynamics by shock wave lithoripsy in pigs,'' Proc. VIII Int'l Symp. Urolithiasis (1996).
[15] D. Dalecki, C. H. Raeman, S. Z. Child, and E. L. Carstensen, ''A test for cavitation as a mechanism for intestinal hemorrhage in mice exposed to a piezoelectric lithotripter,'' Ultrasound Med. Biol. **22**, 493–496 (1996).

[16] C. Hartman, S. Z. Child, R. Mayer, E. Schenk, and E. L. Carstensen, ''Lung damage from exposure to the fields of an electrohydraulic lithotripter,'' Ultrasound Med. Biol. **16**, 675–679 (1990).
[17] A. J. Coleman and J. E. Saunders, ''A review of the physical properties and biological effects of the high amplitude acoustic fields used in extracorporeal lithotripsy,'' Ultrasonics **31**, 75–89 (1993).
[18] D. D. Howard and B. Sturtevant, ''*In vitro* studies of the mechanical effects of shock wave lithotripsy,'' Ultrasound Med. Biol. **23**, 1107–1122 (1997).
[19] A. J. Coleman, M. J. Choi, and J. E. Saunders, ''Theoretical predictions of the acoustic pressure generated by a shock wave lithotripter,'' Ultrasound Med. Biol. **17**, 245–255 (1991).
[20] P. T. Christopher, ''Modeling the Dornier HM3 lithotripter,'' J. Acoust. Soc. Am. **96**, 3088–3095 (1994).
[21] P. T. Christopher and K. J. Parker, ''New approaches to nonlinear diffractive field propagation,'' J. Acoust. Soc. Am. **90**, 488–499 (1991).
[22] E. A. Zabolotskaya and R. V. Khokhlov, ''Quasi-plane waves in the nonlinear acoustics of confined beams,'' Sov. Phys. Acoust. **15**, 35–40 (1969).
[23] V. P. Kuznetsov, ''Equation of nonlinear acoustics,'' Sov. Phys. Acoust. **16**, 467–470 (1970).
[24] A. C. Baker and V. F. Humphrey, ''Distortion and high-frequency generation due to nonlinear propagation of short ultrasonic pulses from a plane circular piston,'' J. Acoust. Soc. Am. **92**, 1699–1705 (1992).
[25] J. A. TenCate, ''An experimental investigation of the nonlinear pressure field produced by a plane circular piston,'' J. Acoust. Soc. Am. **94**, 1084–1089 (1993).
[26] S. Nachef, D. Cathignol, J. Naze Tjøtta, A. M. Berg, and S. Tjøtta, ''Investigation of a high intensity sound beam from a plane transducer: Experimental and theoretical results,'' J. Acoust. Soc. Am. **98**, 2303–2323 (1995).
[27] M. A. Averkiou and M. F. Hamilton, ''Measurements of harmonic generation in a focused finite-amplitude sound beam,'' J. Acoust. Soc. Am. **98**, 3439–3442 (1995).
[28] M. A. Averkiou and M. F. Hamilton, ''Nonlinear distortion of short pulses radiated by plane and focused circular pistons,'' J. Acoust. Soc. Am. **102**, 2539–2548 (1997).
[29] M. A. Averkiou, Y.-S. Lee, and M. F. Hamilton, ''Self-demodulation of amplitude- and frequency-modulated pulses in a thermoviscous fluid,'' J. Acoust. Soc. Am. **94**, 2876–2883 (1993).
[30] E. H. Vefring, J. Naze Tjøtta, and S. Tjøtta, ''Effects of focusing on the nonlinear interaction between two collinear finite amplitude sound beams,'' J. Acoust. Soc. Am. **89**, 1017–1027 (1991).
[31] T. S. Hart and M. F. Hamilton, ''Nonlinear effects in focused sound beams,'' J. Acoust. Soc. Am. **84**, 1488–1496 (1988).
[32] M. A. Averkiou, ''Reflection of focused sound from curved rigid surfaces,'' M.S. thesis, The University of Texas at Austin (1989).
[33] H. T. O'Neil, ''Theory of focusing radiators,'' J. Acoust. Soc. Am. **21**, 516–526 (1949).
[34] M. A. Averkiou, ''Experimental investigation of propagation and reflection phenomena in finite amplitude beams,'' Ph.D. dissertation, The University of Texas at Austin (1994).
[35] F. H. Fenlon and F. S. McKendree, ''Axisymmetric parametric radiation—A weak interaction model,'' J. Acoust. Soc. Am. **66**, 534–547 (1979).
[36] M. F. Hamilton, ''Transient axial solution for the reflection of a spherical wave from a concave ellipsoidal mirror,'' J. Acoust. Soc. Am. **93**, 1256–1266 (1993).
[37] J. Lighthill, *Waves in Fluids* (Cambridge University Press, Cambridge, 1980), pp. 78–83.
[38] D. T. Blackstock, ''Nonlinear acoustics (theoretical),'' in *American Institute of Physics Handbook*, 3rd ed. (McGraw-Hill, New York, 1972), Chap. 3n.
[39] R. O. Cleveland, M. F. Hamilton, and D. T. Blackstock, ''Time-domain modeling of finite-amplitude sound in relaxing fluids,'' J. Acoust. Soc. Am. **99**, 3312–3318 (1996).
[40] Y. S. Lee and M. F. Hamilton, ''Time-domain modeling of pulsed finite-amplitude sound beams,'' J. Acoust. Soc. Am. **97**, 906–917 (1995).
[41] Y.-S. Lee, ''Numerical solution of the KZK equation for pulsed finite amplitude sound beams in thermoviscous fluids,'' Ph. D. dissertation, The University of Texas at Austin (1993).
[42] D. T. Blackstock, ''Connection between the Fay and Fubini solutions for plane sound waves of finite amplitude,'' J. Acoust. Soc. Am. **39**, 1019–1026 (1966).
[43] R. H. Cole, *Underwater Explosions* (Princeton University Press, Princeton, NJ, 1948).
[44] D. T. Blackstock, ''Propagation of a weak shock followed by a tail or arbitrary waveform,'' in *Proceedings of the Eleventh International Congress on Acoustics*, Paris, France, Vol. 1, pp. 305–308 (1983).
[45] C. L. Morfey and F. D. Cotaras, ''Propagation in inhomogeneous medium,'' in *Nonlinear Acoustics*, edited by M. F. Hamilton and D. T. Blackstock (Academic, New York, 1997), Chap. 12.
[46] A. J. Coleman, J. E. Saunders, and M. J. Choi, ''An experimental shock wave generator for lithotripsy studies,'' Phys. Med. Biol. **34**, 1733–1742 (1989).
[47] C. Wurster, J. Staudenraus, and W. Eisenmenger, ''The fibre optic probe hydrophone,'' Proc. 1994 IEEE Ultrson. Symp. Vol. 2, pp. 941–944 (1994).
[48] A. J. Coleman and J. E. Saunders, ''An survey of the acoustic output of commercial extracorporeal shock wave lithotripters,'' Ultrasound Med. Biol. **15**, 213–227 (1989).
[49] M. R. Bailey, ''Control of acoustic cavitation with application to lithotripsy,'' Technical Report ARL-TR-97-1, Applied Research Laboratories, The University of Texas at Austin (1997).
[50] M. R. Bailey, D. T. Blackstock, R. O. Cleveland, and L. A. Crum, ''Comparison of electrohydraulic lithotripters with rigid and pressure-release ellipsoidal reflectors: I. Acoustic field,'' J. Acoust. Soc. Am. **104**, 2517–2524 (1998).
[51] M. R. Bailey, D. T. Blackstock, R. O. Cleveland, and L. A. Crum, ''Comparison of electrohydraulic lithotripters with rigid and pressure-release ellipsoidal reflectors: II. Cavitation fields,'' J. Acoust. Soc. Am. (submitted).
[52] R. O. Cleveland, D. A. Lifshitz, B. A. Connors, A. P. Evan, L. R. Willis, and L. A. Crum, ''*In vivo* pressure measurement of lithotripsy shock waves,'' Ultrasound Med. Biol. **24**, 293–306 (1998).